energy&fuels

pubs.acs.org/EF Article

Lattice-Gas Model for Asphaltene Interactions Observed at Interfaces in the Context of the Yen-Mullins Model

Shaghayegh Darjani, Archana Jagadisan, Joel Koplik, and Sanjoy Banerjee*

Cite This: https://doi.org/10.1021/acs.energyfuels.2c01413 Read Online

ACCESS | Metrics & More | Article Recommendations

ABSTRACT: The presence of asphaltene at both fluid−fluid and fluid−solid interfaces has a wide impact on petroleum recovery processes, for example, by stabilizing oil−gas−water dispersions, adsorbing on reservoir rock surfaces and thus changing their wetting properties, and forming deposits in oil−gas production systems. The Yen-Mullins model for asphaltene behavior in bulk fluids provides a framework for understanding a diverse range of phenomena related to the adsorption dynamics of asphaltene at interfaces and how the adsorbed layers are structured. In this work, we address the relatively less explored parameter, which is accounting for the size and shape of the particles on the interfacial properties and emulsion stability. We discuss our investigations of the asphaltene adsorption and its effects, focusing on oil−water interfaces, and propose a lattice-gas model to explain the experimental observations of the interfacial tension and rheology.

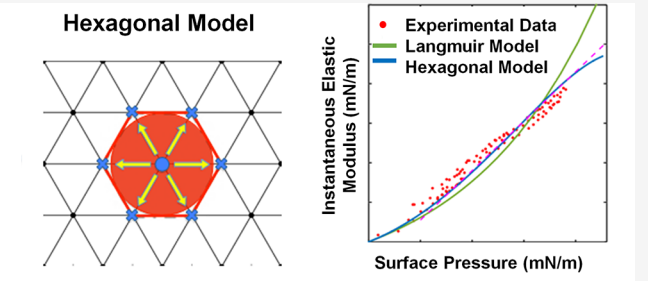

The interfacial effects of adsorbed asphaltenes follow the predictions of the "Hexagonal Lattice Gas Model".

1. INTRODUCTION

Asphaltenes are made of a peripheral alkyl chain attached to polycyclic aromatic hydrocarbon rings[1] and are among the most surface-active and polarizable components of crude oil. They are classified as a solubility class that is soluble in aromatics like toluene but insoluble in *n*-heptane. Molecular structure analysis using atomic force and scanning tunneling microscopy methods shows polydispersed asphaltene with a variety of molecular structures.[2] Following the widely accepted Yen-Mullins model for asphaltene, a molecule's typical molecular weight is about 750 g/mol, and the asphaltene can exist as a monomer, nanoaggregate, or clusters based on their concentration in oil.[1,3]

The stability of crude oil−water emulsions is known to increase with the asphaltene adsorption at an oil−water interface, impacting the process of the oil−water separation and subsequently affecting the oil production.[4,5] The interfacial interaction of the asphaltene-rich crude oil and reservoir rock is also known to influence the reservoir wettability and oil recovery process. Additionally, the precipitation and deposition of asphaltene during various stages of the oil production process can negatively affect the reservoir recovery and result in increased costs because of the downtime in production facilities. Therefore, understanding the interfacial properties of asphaltene is important for the efficient management of petroleum production.

There are several studies focused on understanding the physicochemical effects of asphaltene at interfaces. For the elucidation of the mechanism of adsorption and emulsion stability, a series of experiments using the pendant drop technique covered by asphaltene have been reported.[6−10] A summary of these experimental results are described in the next sections in the context of other studies, which show that many interfacial properties of asphaltene agree with the Langmuir equation of state (EOS). However, there are deviations from the Langmuir model above the surface coverage of ∼65%. We introduce a lattice-gas-based approach to address the limitations of the Langmuir model, which enables us to account for the size and shape of the particles on the interfacial properties of asphaltenes and the emulsion stability. The numerical simulations are in the context of lattice-gas theory; more details can be found in section 3. The bulk composition is related to the composition at the interface using the Gibbs adsorption isotherm.[11]

2. INTERFACIAL EFFECT OF ASPHALTENES AT THE OIL−WATER INTERFACE

2.1. Adsorption Kinetics and Solubility Effect.

Asphaltene adsorption at the oil−water interface results in the decrease of dynamic interfacial tension.[6,10] The interfacial activity depends on the solubility of asphaltenes at the oil−

Special Issue: 2022 Pioneers in Energy Research: Oliver Mullins

Received: May 2, 2022
Revised: July 12, 2022

water interface.[10,12] The interfacial tension rapidly declines initially and varies linearly with the square root of time, indicating a diffusion-controlled adsorption.[6,10,12−16]

For low-solubility asphaltene solutions (asphaltene solutions in mixtures of toluene and aliphatic base oil), the adsorption barrier regime follows the initial diffusion-controlled adsorption because of the steric hindrance effect between already adsorbed molecules. The equilibrium interfacial tension is found to be independent of the asphaltene concentration in an aliphatic oil, and the surface coverage asymptotically reaches the 2D packing limit of polydispersed disks.[6,8] However, for high-solubility asphaltene solution (asphaltene in toluene), the interfacial tension dependent on the asphaltene concentration in the solution and the equilibrium surface coverage can be obtained from the Ward-Tordai equation.[10] Another effect of solubility is that lower surface pressures and higher critical nanoaggregate concentration (CNAC) is obtained in high-solubility asphaltene for the same amount of asphaltene.[10] The equilibrium interfacial tension is reached faster at higher asphaltene concentrations for aromatic solvents and slower for aliphatic solvents,[17] and a lower amount of asphaltene is required to stabilize the emulsion in the aliphatic solvent.[18] However, the surface concentration of ∼4 mg/m^2 is found for the emulsion stability regardless of the asphaltene solubility.[8,18]

2.2. Interfacial Rheology and Equation of State. Particle-laden interfaces between two immiscible liquids can be studied by deformations in the dilatational mode.[19−22] The surface pressure rises as the interfacial layer is compressed because of an increase in the surface concentration. Droplets aged in low-solubility asphaltene solution were rapidly extended until the droplet detachment stage using a pendant droplet apparatus, and the interfacial tension was determined as a function of the interfacial area. The results show that, for asphaltene adsorption, results could be explained by a unique equation of state. The correlation between the surface excess coverage (Γ_∞) and interfacial tension was interpreted by a Langmuir EOS expressed as

$$\gamma(\Gamma) = \gamma_0 + kT\Gamma_\infty \ln(1 - \Gamma/\Gamma_\infty) \quad (1)$$

where γ_0 is the interfacial tension of a clean surface, T is the temperature, and k is the Boltzmann's constant.

The fitting parameter for the Langmuir EOS surface excess coverage was calculated as 3.2 molecules/nm^2, corresponding to the area of the cross section of 0.31 nm^2, which is in agreement with the reported range by Chaverot and co-workers.[15] These results are consistent with the Yen−Mullins model,[1,3] correspond to the average size of the polyaromatic hydrocarbon core of 6−8 rings in asphaltene, and indicate a configuration where alkyl chains orient perpendicularly to the oil phase, and the aromatic cores lie flat at the interface.

The results of the sum frequency generation (SFG) vibrational spectroscopy on the Langmuir−Blodgett film[23] support this interpretation of the asphaltene molecule orientation. Hydrogen bonding between the OH group and the π-electrons of the polycyclic aromatic hydrocarbons rings leads to the flat adsorption of the polyaromatic hydrocarbon core at the interface.[24] The results of SFG are confirmed by the coarse-grained molecular simulation using dissipative particle dynamics (DPD) for different initial molecular orientations. The coarse-grained model shows that asphaltene molecules remain parallel to the interface, even at a high surface coverage.[25]

The applicability of the Langmuir EOS is also established for petroleum-derived asphaltene extracted from Kuwaiti UG8, coal-derived, and synthetic asphaltene. Analysis of the surface excess coverage for petroleum-derived, coal-derived, and synthetic asphaltene yielded an approximately 6-ring core, 4-ring core, and a 13-ring core, respectively. Estimates of the average ring size in the polyaromatic core obtained from interfacial property measurements are consistent with the understanding from other studies,[23,26] proving the validity of the Langmuir EOS for the adsorption of asphaltene derived from a range of materials.

2.3. Mechanism for Coalescence Blocking. When emulsions are left at rest or gently stirred, the coalescence process continues until the surface concentration reaches a significant value of approximately 4 mg/m^2. This critical value of surface concentration is found to be independent of adsorption properties such as the bulk concentration or the nature of the solvent.[27−30]

The rapid increase and decrease in asphaltene concentrations occurring during coalescence events is simulated using the pendant drop experiments through rapidly contracting and expanding asphaltene-laden interfaces.[9] Until surface pressure values of ∼21 mN/m, contraction curves for droplets aged in asphaltene solutions follow the Langmuir EOS (Figure 1),

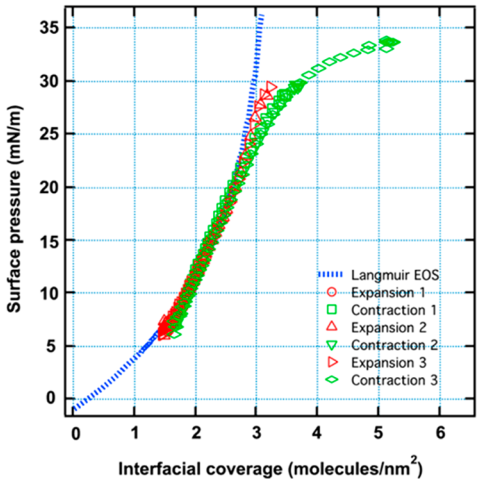

Figure 1. Surface pressure vs interfacial coverage for contraction/expansion experiments. Reproduced with permission from ref 9. Copyright 2014 American Chemical Society.

beyond which the contraction curves deviate from the Langmuir EOS. At this point the droplet shows solidlike behavior on the surface as it does not conform to the shape predicted by the Young−Laplace equation. Further contractions cause wrinkles to develop, which disappear in a short time, which is thought to be the result of gradual desorption followed by a change to a glassy surface. This happens when the contraction exceeds a packing limit of ∼85%. The surface pressure versus interfacial coverage for expansion and contraction experiments is shown in Figure 1. The findings demonstrate that there does not appear to be aging, cross-linking, or gelation at the interface as all the curves fall onto the same Langmuir EOS curve for a surface pressure value of approximately 21 mN/m.

An alternative school of thought is that the formation of the gel through a physically cross-linked network of asphaltene

https://doi.org/10.1021/acs.energyfuels.2c01413
Energy Fuels XXXX, XXX, XXX−XXX

prevents a coalescence.[4,5,19,30−34] Gel point rheology is supported by the experimental observation that the shear elasticity increase is correlated with the chemical condition and aging time, causing emulsion stability.[20,35] Alicke and co-workers find that the packing of the asphaltene nanoaggregate is responsible for the emulsion stability.[36]

Interfacial rheology is shown to be correlated with the emulsion stability and is a better indication of stabilization than interfacial tension reduction.[37,38] The emulsion stability occurs because of the mechanical resistance to coalescence,[38] where the magnitude of elasticity depends on the asphaltene molecular structure. The result of the interfacial shear rheology shows that the bulk concentration and aging time are increased, and the interface becomes more elastic.[20,35]

It is reported that the shear elasticity increases suddenly with an increase in the asphaltene mass fraction, whereas the dilatational elastic modulus levels off by increasing the concentration before a sharp decline.[31,35,36,39−41] This observation is in contrast with gel point rheology, where decreasing the modulus by increasing the concentration is unexpected.[21]

2.4. Reversibility of Asphaltene Adsorption and Polydispersity of Asphaltene. Observations from contraction experiments of the droplet aged with asphaltene left at rest indicate a relaxation toward higher interfacial tensions until values similar to those before the compression are approached and the wrinkles formed on contraction also disappear after some time, suggesting the partial desorption of asphaltene from the interface.[9,10] The coarse-grained model coupled with dissipative particle dynamics (DPD) also shows that, at high surface coverage, some asphaltene molecules desorbed into the oil region because of the steric hindrance between adsorbed particles.[25] The investigation of surfactants and proteins indicate that the desorption kinetics are dependent on the surface activity of the materials,[42,43] and the more surface-active the surfactant, the slower the desorption.

Many studies have shown that a small fraction of the asphaltene is surface-active, indicating that a fraction of the overall bulk concentration is responsible for the emulsion stability.[4,15,21,30,39] The surface-active fraction depends on the source of asphaltene and could vary from 2 to 65%.[30] It was observed that when the most surface-active subfraction is removed, the interfacial tension increases, emulsion gradually becomes less stable regardless of the asphaltene origin,[30] and the less soluble fraction is found to be the strongest stabilizer.[30,34]

3. LATTICE GAS ADSORPTION OF ASPHALTENE AT OIL−WATER INTERFACES

Molecular ordering at interfaces determines the ability of a surface-active agent to bring dissimilar materials such as oil and water together at the microscopic scale where these materials prefer to be phase-separated on a macroscopic scale.[44] Adsorption of asphaltene at the oil−water interface is thermodynamically favorable, but the adsorption process can be kinetically limited because of the presence of an adsorption barrier.[45] The adsorption of asphaltene at the oil−water interface can be considered a multistage process. In the first stage, asphaltene will transfer from the bulk solution to the vicinity of the interface, the so-called subsurface layer. In the second stage, adsorption of asphaltene from the subsurface to the interface will occur, which can lead to the formation of a monolayer. The same approach is widely used for the adsorption of protein[46] and surfactant in the literature. The first step can be due to convection or diffusion.[46] The schematic of the adsorption of asphaltene at the oil−water interface below the critical nanoaggregation concentrations is presented in Figure 2.

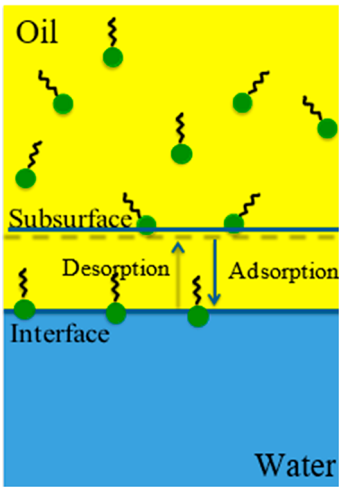

Figure 2. Adsorption of asphaltene from the oil phase to the interface.

In the pendant drop experiment, the asphaltene diffuses to the subsurface layer initially:

$$\frac{\partial C(r,t)}{\partial t} = \frac{D}{r^2}\frac{\partial}{\partial r}\left(r^2\frac{\partial c}{\partial r}(r,t)\right),\ b < r < B,\ t > 0 \tag{2}$$

with the boundary condition

$$c(B,t) = c_b,\ t > 0 \tag{3}$$

$$\frac{\mathrm{d}\Gamma}{\mathrm{d}t} = D\frac{\partial c}{\partial r}(b,t),\ \ t > 0 \tag{4}$$

and initial condition:

$$\Gamma(0) = 0 \tag{5}$$

$$c(b,0) = 0 \tag{6}$$

$$c(r,0) = c_b,\ \ b < r \le B \tag{7}$$

where Γ is the surface concentration and b and B refer to the subsurface layer and the bulk, respectively. To solve the diffusion equation, we need to know the surface concentration (which is unknown in the pendant drop experiment), and we also need to do kinetic modeling for the adsorption process from the subsurface layer to the interface. The relationship between the surface concentration and surface area is obtained from the expansion−contraction experiment, as explained in the previous subsections.

3.1. Choice of Lattice-Gas Model. The numerical simulation is performed based on the triangular lattice with nearest-neighbor exclusion. This model chosen for exploration here is based on the geometry of coronene and estimated molecular area found from the Langmuir model, as illustrated in Figure 3. The coronene molecule has seven fused aromatic rings. Each fused benzenoid ring is represented by a bead, so each coronene is represented by seven beads.

We recently developed a new approach using the random sequential adsorption model (RSAD) with surface diffusion to obtain the equation of state of 2D hard-core particles based on

https://doi.org/10.1021/acs.energyfuels.2c01413
Energy Fuels XXXX, XXX, XXX−XXX

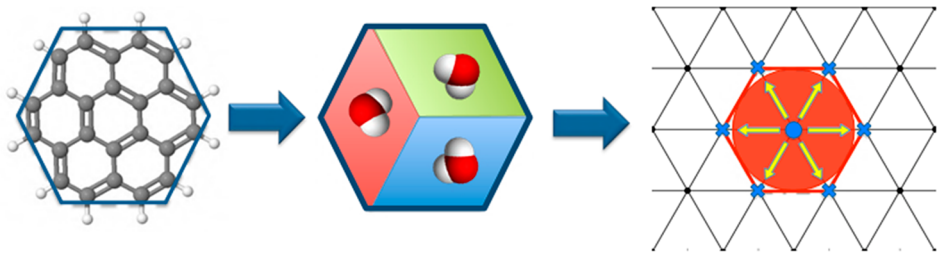

(a) (b) (c)

Figure 3. (a) Molecular structure of coronene. (b) Each asphaltene covers three water molecules. (c) Choice of lattice-gas model: Triangular lattice with nearest-neighbor exclusion (the "hexagonal" model).

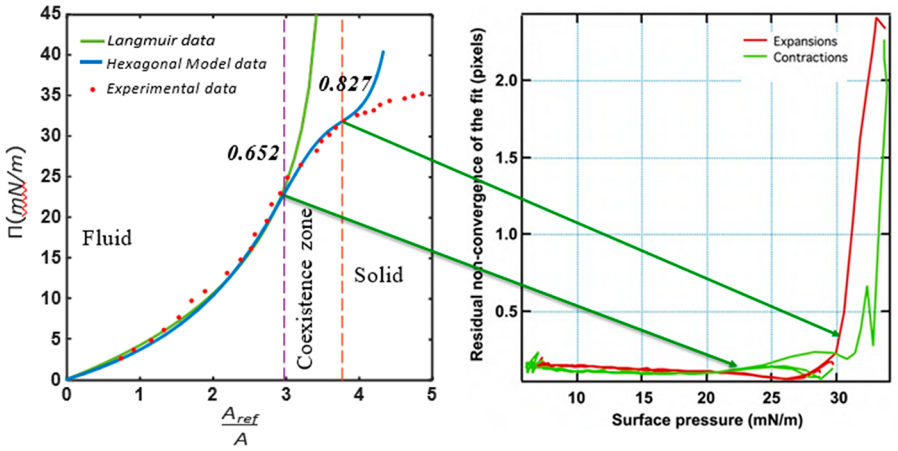

(a) (b)

Figure 4. (a) Comparison of the hexagonal model with experimental results obtained from the compression and expansion experiment in a poor solvent; (b) residual nonconvergence of the fit with Laplacian shape. Reproduced with permission from ref 9. Copyright 2014 American Chemical Society.

the Gibbs adsorption isotherm and kinetic arguments.[47−49] With use of this approach, for equilibrium between a 2D lattice gas with a 3D solution of adsorbate molecules, the equality of the chemical potential all through the system leads to the following relation for the surface pressure (Π),

$$d\Pi = kT\frac{\Theta}{A_a}\, d\ln C \tag{8}$$

Here, k is Boltzmann's constant, C is the total concentration of the solution, A_a is the interfacial area covered by a single adsorbate, T is the temperature, and Θ is the total fractional surface coverage. Integration of the above equation leads to

$$\int_0^{\Theta} \frac{\Theta}{C}\frac{\partial C}{\partial \Theta}\, d\Theta = \frac{A_a}{kT}\Pi \tag{9}$$

Here, we see that the EOS, Π(Θ), can be calculated using information on the adsorption isotherm and the relationship among $C(\Theta)$, the fractional coverage, and the bulk concentration. Kinetic arguments for each species can be used to obtain the adsorption isotherm. The desorption and adsorption rates of each species are the same at equilibrium; therefore,

$$K_{a_i} C_{b_i}\left(1 - \beta\left(\sum \Theta_i\right)\right) = K_{d_i}\Theta_i \tag{10}$$

where K_{a_i} is the adsorption rate constant and K_{d_i} the desorption rate constant of species i, $\beta(\sum\Theta_i)$ is the fraction of the surface area excluded from further adsorption by already adsorbed particles, the "blocking function", and C_{b_i} is the bulk concentration of species i. Solving for C and substituting into the integral version of the Gibbs adsorption isotherm yields

$$\int_0^{\Theta} (1 - \beta(\Theta))\frac{\partial}{\partial\Theta}\left[\frac{\Theta}{1 - \beta(\Theta)}\right] d\Theta = \frac{A_a}{kT}\Pi \tag{11}$$

where $\Theta = \sum\Theta_i$. The blocking function, which may be obtained through RSAD simulations, is the only piece of information required to compute the equation of state. From the definition of the adsorption rate,

$$\frac{\partial\Theta_1}{\partial t} = \frac{K_{l_1}}{r}\left(1 - \beta\left(\sum\Theta_i\right)\right) - \frac{\Theta_1}{r} \tag{12}$$

$$\frac{\partial\Theta_2}{\partial t} = \frac{K_{l_1}}{\alpha r}\left(1 - \beta\left(\sum\Theta_i\right)\right) - \frac{K_{l_1}\Theta_1}{\alpha K_{l_2} r} \tag{13}$$

$$\frac{\partial\Theta}{\partial t} = \frac{\partial\Theta_1}{\partial t} + \frac{\partial\Theta_2}{\partial t} \tag{14}$$

where $K_{l_i} = C_{b_i}K_{a_i}/K_{d_i}$ is the ratio of the adsorption-to-desorption attempt of species i, $t = nA_a/A$, n is the number of attempts, $r = 1 + K_{l_1} + K_{l_1}/\alpha + K_{l_1}/(\alpha K_{l_2})$, and the effective adsorption ratio $\alpha = K_{a_1}C_{b_1}/(K_{a_2}C_{b_2})$.

https://doi.org/10.1021/acs.energyfuels.2c01413
Energy Fuels XXXX, XXX, XXX−XXX

Figure 3b shows the adsorption of molecules covering three adsorption sites, which is the outcome of the adsorption of hard-core molecules along with first neighbor exclusion. A periodic boundary condition is used to mitigate the effects of finite size in the adsorption method, which involves gradually adding molecules or particles to an originally empty lattice surface. Because of the assumption of steric limitation, the restriction is that overlap is not permitted. A random point (x,y) representing the particle's center of mass is chosen for each attempt at adsorption. Adsorption is accepted if both the chosen site and its neighbors are vacant; otherwise, it is rejected. Diffusion is introduced sequentially, which is the simultaneous movement of particles. A particle that was adsorbed earlier and a displacement direction for the particle are chosen randomly for every diffusion attempt. Diffusion is accepted if moving the center of mass of that particle to the next node along this chosen direction does not violate the nonoverlap condition. Upon the fast surface diffusion, the surface layer is at internal equilibrium, even in the case of transient adsorption and the blocking function can be considered as a state function.

Desorption is incorporated into the system with identical binary species, which have the same size and shape, but different K_l's. A particle gets removed in a desorption attempt if it has the same type as the randomly selected species and if a chosen site lies inside the adsorbed particle. If not, we choose one of the six nearby sites at random and remove the particle if it is related to the center of mass of an adsorbate with the same type. Or else the attempt is denied. To obtain the blocking function and to the extract the success rate, we performed 1500 independent runs. Previous experimental data for interfacial interactions between water and the solution of asphaltene is re-analyzed in the following section.

3.2. Results. *3.2.1. Comparison between the Hexagonal Model and Compression–Expansion Experiment.* Previous compression–expansion experimental data[9] are re-analyzed with a hexagonal model, as shown in Figure 4a. The residual nonconvergence of the fit from a Laplacian shape (r) is presented in Figure 4b and can be calculated as

$$r = \sqrt{\frac{\text{ersum}}{m}} \tag{15}$$

where "ersum" is the summation of the square orthogonal distance (in pixels) between the detected edge point and the Young–Laplace equation and m is the number of detected points.

Although the Langmuir model can predict the experimental data fairly well at low surface coverage, it deviates from experimental data at higher coverage around 23 mN/m surface pressure where some fluctuation is also observed in the residual nonconvergence of the fit from the Laplacian shape, as illustrated in Figure 4b. This value of surface pressure is equivalent to the entrance to the coexisting zone found in the hexagonal model (illustrated in Figure 4a). As a result, the Langmuir EOS is able to predict the adsorption behavior of asphaltene fairly well in the fluid regime.

Upon further contraction, wrinkles appear on the droplet aged with asphaltene solution, which also are explained by the hexagonal model. A large deviation from the Laplacian shape is observed around 32 mN/m, which is equivalent to the prediction of the hexagonal model about the entrance to the solidification zone. Our results indicate[47−49] that a sharp transition occurs from the disorder regime to the order regime at solidification coverage. The average molecular weight of asphaltene is 750 g/mol, so the packing fraction of the hexagonal model corresponds to 3.86 mg/m^2 surface concentration, which is in the reported range for emulsion stability obtained from the experiment.[28,9] Birefringence is also observed by Varadaraj and co-worker[50] upon contracting the aged droplet using cross-polarized light microscopy, which confirms the ordering of the monolayer at high concentration.

For wrinkles to be observed on the droplet aged with asphaltene solution, the coverage should reach the jamming or solidification coverage. In the experiment performed by Zarkar and co-workers,[10] no wrinkles were observed because the surface pressure after the compression experiment was 13 mN/m, where this surface pressure corresponds to the liquid regime in the hexagonal model.

Our new model could explain hysteresis between contraction and expansion experiments. Because of the rapid compression of the monolayer, the system does not relax completely to a new equilibrium state, which causes kinetic frustration, and hysteresis is observed between compression (adsorption method in the hexagonal model) and expansion (desorption method in the hexagonal model).[47,51] Because of the presence of hysteresis between the compression and expansion experiment, we expect that the droplet relaxes down to a lower surface pressure based on our model. It is experimentally observed that when the contracted droplet is left at rest, wrinkles disappeared and the surface pressure relaxed down to the value before the contraction experiment.[9]

Our results indicate[48,51] that, at very low surface diffusion, rapid monolayer compression forces the system toward a locked or metastable configuration. At high concentrations, the in-plane rearrangement of particles due to the compression becomes too difficult and leads to the appearance of viscoelasticity in the monolayer.[38] This system has many phenomenological characteristics that are qualitatively similar to those of supercooled liquids and glasses. The system gets stuck in a metastable state and will only gradually relax toward equilibrium. The caging effect at high surface coverage can be relaxed with thermal motion or stress, which has the same concept as the soft glass rheology model (SGR). This model is used to explain the shear rheology experimental data.[9,36,38]

3.2.2. Comparison between the Hexagonal Model and Dilatational Rheology Experiments. Dilatational rheology versus the surface pressure of a solution of asphaltene in a poor solvent in the oil–water interface from Rane and co-workers[7] is re-analyzed by the hexagonal model. Instantaneous elastic modulus, E_0, is equivalent to compressibility (κ) in lattice-gas theory and can be determined through the following equation: $E_0 = \frac{1}{\kappa} = \Theta\left(\frac{\partial \Pi}{\partial \Theta}\right)_T$. Although the Langmuir model can predict the experimental data at low surface pressure reasonably well, with increasing surface pressure the Langmuir EOS deviates from the experimental data, as presented in Figure 5. However, the hexagonal model is able to predict the experimental data in the whole range and also more precisely. Instantaneous elastic modulus, E_0, changes linearly by increasing the surface pressure and passes through a maxima followed by a sharp decrease. This trend is also reported for the adsorption of a surfactant.[52,53]

3.2.3. Comparison between Hexagonal Model and Dynamic Interfacial Tension Experiment. We previously showed that the adsorption of asphaltene in toluene followed the binary diffusional model.[21] Here, we compare the dynamic

https://doi.org/10.1021/acs.energyfuels.2c01413
Energy Fuels XXXX, XXX, XXX−XXX

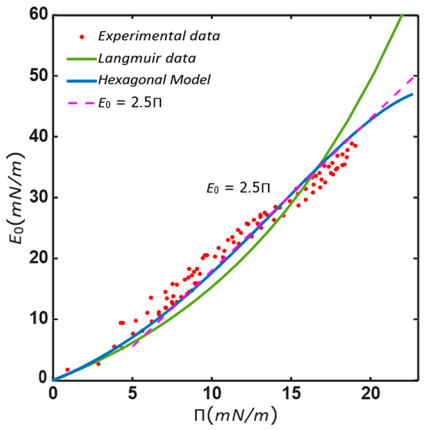

Figure 5. Comparison between the hexagonal model and dilatational rheology experiment in a poor solvent. The experimental data is obtained from Rane et al.[7]

interfacial tension of the hexagonal model with experimental results of 0.5 and 1 kg/m^3 of asphaltene in toluene[39] in Figure 6. The same bulk concentrations and adsorption coefficients are used as in our previous paper.[21] The hexagonal model could precisely predict the experimental results. Our results confirm that only a small fraction of asphaltene as low as 8% are surface-active in toluene. The most surface-active component is less than 0.5% of the bulk concentration, where this amount is consistent with the amount of asphaltene responsible for the emulsion stability.[4,54]

Figure 6b shows the results plotted in a linear time scale. The simulations results are within the range of experimental error (±0.5 mN/m). Initially, the interfacial tension decreases rapidly and varies linearly with the square root of time, indicating a diffusion-controlled adsorption. With an increase in surface coverage, the area left free for further adsorption decreases because (i) the sites are occupied by formerly adsorbed asphaltenes and (ii) the vacancies can be too small for adsorption without overlap. A denser, more organized monolayer results from diffusional relaxation on the surface.

4. CONCLUSION

The interfacial effects of adsorbed asphaltene follow the hexagonal model EOS. The adsorption of asphaltene at the oil−water interface can be explained over the whole range of observations using a lattice-gas approach and are consistent with the aggregation behavior of asphaltenes in the bulk fluid and asphaltene average core size expected from the Yen−Mullins model.

The Gibbs elasticity (E_0) rises linearly by increasing the surface pressure and passes through a maxima followed by a sharp decrease. This observation merges the mechanical resistance against compaction of the interface.

The lattice-gas model predicts that the asphaltene-laden oil−water interface undergoes a fluid-to-solid transition because of the steric hindrance between the adsorbed particles at 85% surface coverage where the rise of shear elasticity is expected. At this coverage, a sharp deviation from the Laplacian shape is observed on the residual nonconvergence of the fit with the Laplacian shape. On the basis of this model, the ordering parameter increases sharply at the solidification coverage, which is consistent with the experimental observation of birefringence on the contracting droplet aged with asphaltene.

Because of the rapid compression of the monolayer, the system does not relax completely to a new equilibrium state, which causes kinetic frustration in the system, and hysteresis is observed between the compression and expansion experiment. The system could be pushed toward a locked or metastable configuration, where the system behaves like a glass, in the case of very rapid compression of the monolayer. Indeed, a soft glass rheology model could be used to explain the shear behavior of such a system.

The packing fraction of the hexagonal model (shown in Figure 4) corresponds to a 3.86 mg/m^2 surface concentration of asphaltene. This surface concentration is consistent with the critical value (3.6−3.9 mg/m^2) experimentally observed for the emulsion stability. Our results suggest that the lattice-gas approach can reliably address the limitations of the Langmuir model, including the observations of fluid−solid transitions at a high surface coverage, which are important in better understanding the role of asphaltene in stabilizing oil−water emulsions.

AUTHOR INFORMATION

Corresponding Author

Sanjoy Banerjee − *Energy Institute and Department of Chemical Engineering, City College of New York, New York, New York 10031, United States;* orcid.org/0000-0002-3128-8559; Email: banerjee@che.ccny.cuny.edu

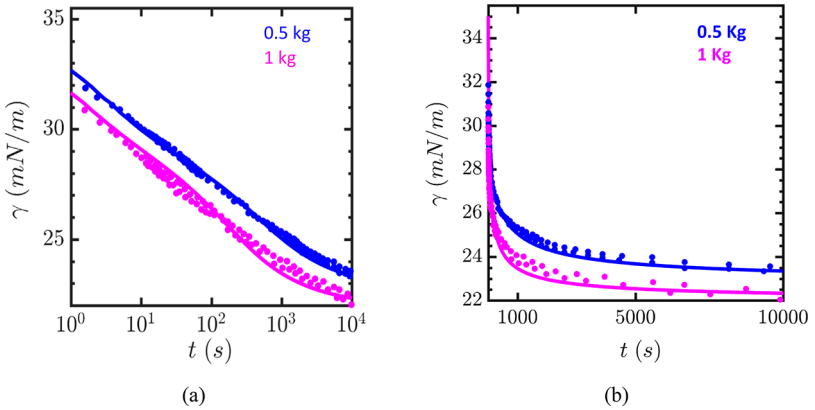

Figure 6. Comparison between the hexagonal model and dynamic interfacial tension: the solid line represents the hexagonal model, and solid circles represent the experimental data. (a) Plotted on an exponential time scale. (b) Plotted on a linear time scale. The experimental data are obtained from Sztukowski and Yarranton.[39]

https://doi.org/10.1021/acs.energyfuels.2c01413
Energy Fuels XXXX, XXX, XXX−XXX

Authors

Shaghayegh Darjani − *Energy Institute and Department of Chemical Engineering, City College of New York, New York, New York 10031, United States*

Archana Jagadisan − *Energy Institute and Department of Chemical Engineering, City College of New York, New York, New York 10031, United States*

Joel Koplik − *Levich Institute and the Department of Physics, City College of New York, New York, New York 10031, United States*

Complete contact information is available at: https://pubs.acs.org/10.1021/acs.energyfuels.2c01413

Notes

The authors declare no competing financial interest.

■ ACKNOWLEDGMENTS

This research was supported by the National Science Foundation under Grant No. 1743794, PIRE: Investigation of Multi-Scale, Multi-Phase Phenomena in Complex Fluids for the Energy Industries.

■ REFERENCES

(1) Mullins, O. C.; Sabbah, H.; Eyssautier, J.; Pomerantz, A. E.; Barre, L.; Andrews, A. B.; Ruiz-Morales, Y.; Mostowfi, F.; McFarlane, R.; Goual, L.; et al. Advances in Asphaltene Science and the YenMullins Model. *Energy Fuels* **2012**, *26* (7), 3986−4003.

(2) Schuler, B.; Meyer, G.; Peña, D.; Mullins, O. C.; Gross, L. Unraveling the molecular structures of asphaltenes by atomic force microscopy. *J. Am. Chem. Soc.* **2015**, *137* (31), 9870−9876.

(3) Mullins, O. C. The Modified Yen Model. *Energy Fuels* **2010**, *24* (4), 2179−2207.

(4) Yang, F.; Tchoukov, P.; Pensini, E.; Dabros, T.; Czarnecki, J.; Masliyah, J.; Xu, Z. Asphaltene subfractions responsible for stabilizing water-in-crude oil emulsions. Part 1: interfacial behaviors. *Energy Fuels* **2014**, *28* (11), 6897−6904.

(5) Kilpatrick, P. K. Water-in-crude oil emulsion stabilization: review and unanswered questions. *Energy Fuels* **2012**, *26* (7), 4017−4026.

(6) Rane, J. P.; Harbottle, D.; Pauchard, V.; Couzis, A.; Banerjee, S. Adsorption kinetics of asphaltenes at the oil−water interface and nanoaggregation in the bulk. *Langmuir* **2012**, *28* (26), 9986−9995.

(7) Rane, J. P.; Pauchard, V.; Couzis, A.; Banerjee, S. Interfacial rheology of asphaltenes at oil-water interfaces and interpretation of the equation of state. *Langmuir* **2013**, *29*, 4750−4759.

(8) Pauchard, V.; Rane, J. P.; Zarkar, S.; Couzis, A.; Banerjee, S. Long-Term Adsorption Kinetics of Asphaltenes at the Oil−Water Interface: A Random Sequential Adsorption Perspective. *Langmuir* **2014**, *30*, 8381−8390.

(9) Pauchard, V.; Rane, J. P.; Banerjee, S. Asphaltene-laden interfaces form soft glassy layers in contraction experiments: A mechanism for coalescence blocking. *Langmuir* **2014**, *30* (43), 12795−12803.

(10) Zarkar, S.; Pauchard, V.; Farooq, U.; Couzis, A.; Banerjee, S. Interfacial Properties of Asphaltenes at Toluene - Water Interfaces. *Langmuir* **2015**, *31*, 4878−4886.

(11) Pradilla, D.; Simon, S.; Sjöblom, J. Mixed interfaces of asphaltenes and model demulsifiers part I: Adsorption and desorption of single components. *Colloids Surf., A* **2015**, *466*, 45−56.

(12) Fossen, M.; Kallevik, H.; Knudsen, K. D.; Sjöblom, J. Asphaltenes precipitated by a two-step precipitation procedure. 1. Interfacial tension and solvent properties. *Energy Fuels* **2007**, *21* (2), 1030−1037.

(13) Liu, D.; Li, C.; Yang, F.; Sun, G.; You, J. Adsorption behavior and interfacial dilational properties of asphaltenes at the interface between n-decane/α-methylnaphthalene and brine water. *J. Dispersion Sci. Technol.* **2020**, *41* (6), 918−928.

(14) Zhang, S.; Zhang, L.; Lu, X.; Shi, C.; Tang, T.; Wang, X.; Huang, Q.; Zeng, H. Adsorption kinetics of asphaltenes at oil/water interface: Effects of concentration and temperature. *Fuel* **2018**, *212*, 387−394.

(15) Chaverot, P.; Cagna, A.; Glita, S.; Rondelez, F. Interfacial tension of bitumen− water interfaces. Part 1: Influence of endogenous surfactants at acidic pH. *Energy Fuels* **2008**, *22* (2), 790−798.

(16) You, J.; Li, C.; Liu, D.; Yang, F.; Sun, G. Influence of the aggregation state of asphaltenes on structural properties of the model oil/brine interface. *Energy Fuels* **2019**, *33* (4), 2994−3002.

(17) Jeribi, M.; Almir-Assad, B.; Langevin, D.; Henaut, I.; Argillier, J. F. Adsorption kinetics of asphaltenes at liquid interfaces. *J. Colloid Interface Sci.* **2002**, *256* (2), 268−272.

(18) Gafonova, O. V.; Yarranton, H. W. The stabilization of water-in-hydrocarbon emulsions by asphaltenes and resins. *J. Colloid Interface Sci.* **2001**, *241* (2), 469−478.

(19) Freer, E. M.; Radke, C. J. Relaxation of asphaltenes at the toluene/water interface: diffusion exchange and surface rearrangement. *J. Adhes.* **2004**, *80* (6), 481−496.

(20) Fan, Y.; Simon, S.; Sjöblom, J. Interfacial shear rheology of asphaltenes at oil−water interface and its relation to emulsion stability: Influence of concentration, solvent aromaticity and nonionic surfactant. *Colloids Surf., A* **2010**, *366* (1−3), 120−128.

(21) Liu, F.; Darjani, S.; Akhmetkhanova, N.; Maldarelli, C.; Banerjee, S.; Pauchard, V. Mixture effect on the dilatation rheology of asphaltenes-laden interfaces. *Langmuir* **2017**, *33* (8), 1927−1942.

(22) Kotula, A. P.; Anna, S. L. Insoluble layer deposition and dilatational rheology at a microscale spherical cap interface. *Soft Matter* **2016**, *12* (33), 7038−7055.

(23) Andrews, A. B.; McClelland, A.; Korkeila, O.; Demidov, A.; Krummel, A.; Mullins, O. C.; Chen, Z. Molecular orientation of asphaltenes and PAH model compounds in Langmuir− Blodgett films using sum frequency generation spectroscopy. *Langmuir* **2011**, *27* (10), 6049−6058.

(24) Meszar, Z. E.; Hantal, G.; Picaud, S.; Jedlovszky, P. Adsorption of aromatic hydrocarbon molecules at the surface of ice, as seen by grand canonical Monte Carlo simulation. *J. Phys. Chem. C* **2013**, *117* (13), 6719−6729.

(25) Ruiz-Morales, Y.; Mullins, O. C. Coarse-grained molecular simulations to investigate asphaltenes at the oil−water interface. *Energy Fuels* **2015**, *29* (3), 1597−1609.

(26) Groenzin, H.; Mullins, O. C. Molecular Size and Structure of Asphaltenes from Various Sources. *Energy Fuels* **2000**, *14* (3), 677−684.

(27) Pauchard, V.; Roy, T. Blockage of coalescence of water droplets in asphaltenes solutions: A jamming perspective. *Colloids and Surfaces A: Physicochemical and Engineering Aspects.* **2014**, *443*, 410−417.

(28) Yarranton, H. W.; Hussein, H.; Masliyah, J. H. Water-in-hydrocarbon emulsions stabilized by asphaltenes at low concentrations. *J. Colloid Interface Sci.* **2000**, *228* (1), 52−63.

(29) Rocha, J. A.; Baydak, E. N.; Yarranton, H. W.; Sztukowski, D. M.; Ali-Marcano, V.; Gong, L.; Shi, C.; Zeng, H. Role of aqueous phase chemistry, interfacial film properties, and surface coverage in stabilizing water-in-bitumen emulsions. *Energy Fuels* **2016**, *30* (7), 5240−5252.

(30) Rocha, J. A.; Baydak, E. N.; Yarranton, H. W. What fraction of the asphaltenes stabilizes water-in-bitumen emulsions? *Energy Fuels* **2018**, *32* (2), 1440−1450.

(31) Yarranton, H. W.; Sztukowski, D. M.; Urrutia, P. Effect of interfacial rheology on model emulsion coalescence: I. interfacial rheology. *J. Colloid Interface Sci.* **2007**, *310* (1), 246−252.

(32) McLean, J. D.; Kilpatrick, P. K. Effects of asphaltene solvency on stability of water-in-crude-oil emulsions. *J. Colloid Interface Sci.* **1997**, *189* (2), 242−253.

(33) Verruto, V. J.; Kilpatrick, P. K. Water-in-model oil emulsions studied by small-angle neutron scattering: interfacial film thickness and composition. *Langmuir* **2008**, *24* (22), 12807−12822.

(34) Spiecker, P. M.; Kilpatrick, P. K. Interfacial rheology of petroleum asphaltenes at the oil−water interface. *Langmuir* **2004**, *20* (10), 4022−4032.
(35) Harbottle, D.; Chen, Q.; Moorthy, K.; Wang, L.; Xu, S.; Liu, Q.; Sjoblom, J.; Xu, Z. Problematic stabilizing films in petroleum emulsions: Shear rheological response of viscoelastic asphaltene films and the effect on drop coalescence. *Langmuir* **2014**, *30* (23), 6730−6738.
(36) Alicke, A.; Simon, S.; Sjöblom, J.; Vermant, J. Assessing the interfacial activity of insoluble asphaltene layers: Interfacial rheology versus interfacial tension. *Langmuir* **2020**, *36* (49), 14942−14959.
(37) Dicharry, C.; Arla, D.; Sinquin, A.; Graciaa, A.; Bouriat, P. Stability of water/crude oil emulsions based on interfacial dilatational rheology. *J. Colloid Interface Sci.* **2006**, *297* (2), 785−791.
(38) Samaniuk, J. R.; Hermans, E.; Verwijlen, T.; Pauchard, V.; Vermant, J. Soft-glassy rheology of asphaltenes at liquid interfaces. *J. Dispersion Sci. Technol.* **2015**, *36* (10), 1444−1451.
(39) Sztukowski, D. M.; Yarranton, H. W. Rheology of asphaltene−toluene/water interfaces. *Langmuir* **2005**, *21* (25), 11651−11658.
(40) Alvarez, G.; Poteau, S.; Argillier, J. F.; Langevin, D.; Salager, J. L. Heavy oil− water interfacial properties and emulsion stability: Influence of dilution. *Energy Fuels* **2009**, *23* (1), 294−299.
(41) Angle, C. W.; Hua, Y. Dilational interfacial rheology for increasingly deasphalted bitumens and n-C5 asphaltenes in toluene/NaHCO3 solution. *Energy Fuels* **2012**, *26* (10), 6228−6239.
(42) Fainerman, V. B.; Leser, M. E.; Michel, M.; Lucassen-Reynders, E. H.; Miller, R. Kinetics of the desorption of surfactants and proteins from adsorption layers at the solution/air interface. *J. Phys. Chem. B* **2005**, *109* (19), 9672−9677.
(43) Spiecker, P. M.; Gawrys, K. L.; Kilpatrick, P. K. Aggregation and solubility behavior of asphaltenes and their subfractions. *J. Colloid Interface Sci.* **2003**, *267* (1), 178−193.
(44) Tikhonov, A. M.; Pingali, S. V.; Schlossman, M. L. Molecular ordering and phase transitions in alkanol monolayers at the water−hexane interface. *J. Chem. Phys.* **2004**, *120* (24), 11822−11838.
(45) Bizmark, N.; Ioannidis, M. A.; Henneke, D. E. Irreversible adsorption-driven assembly of nanoparticles at fluid interfaces revealed by a dynamic surface tension probe. *Langmuir* **2014**, *30* (3), 710−717.
(46) Adamczyk, Z. Modeling adsorption of colloids and proteins. *Curr. Opin. Colloid Interface Sci.* **2012**, *17* (3), 173−186.
(47) Darjani, S.; Koplik, J.; Pauchard, V. Extracting the equation of state of lattice gases from random sequential adsorption simulations by means of the Gibbs adsorption isotherm. *Phys. Rev. E* **2017**, *96* (5), 052803.
(48) Darjani, S. Adsorption Kinetics and Phase Behavior of Particles Adsorbed at an Interface. Ph.D. Dissertation. The City College of New York, New York, 2021.
(49) Darjani, S.; Koplik, J.; Pauchard, V.; Banerjee, S. Adsorption kinetics and thermodynamic properties of a binary mixture of hard-core particles on a square lattice. *J. Chem. Phys.* **2021**, *154* (7), 074705.
(50) Varadaraj, R.; Brons, C. Molecular origins of crude oil interfacial activity. Part 4: oil−water interface elasticity and crude oil asphaltene films. *Energy Fuels* **2012**, *26* (12), 7164−7169.
(51) Darjani, S.; Koplik, J.; Pauchard, V.; Banerjee, S. Glassy dynamics and equilibrium state on the honeycomb lattice: Role of surface diffusion and desorption on surface crowding. *Phys. Rev. E* **2021**, *103* (2), 022801.
(52) Benjamins, J.; Lyklema, J.; Lucassen-Reynders, E. H. Compression/expansion rheology of oil/water interfaces with adsorbed proteins. Comparison with the air/water surface. *Langmuir* **2006**, *22* (14), 6181−6188.
(53) Fainerman, V. B.; Kovalchuk, V. I.; Aksenenko, E. V.; Michel, M.; Leser, M. E.; Miller, R. Models of two-dimensional solution assuming the internal compressibility of adsorbed molecules: a comparative analysis. *J. Phys. Chem. B* **2004**, *108* (36), 13700−13705.
(54) Xu, Y.; Dabros, T.; Hamza, H.; Shefantook, W. Destabilization of water in bitumen emulsion by washing with water. *Petroleum Science Technology* **1999**, *17* (9−10), 1051−1070.

https://doi.org/10.1021/acs.energyfuels.2c01413
Energy Fuels XXXX, XXX, XXX−XXX